Supplementary Material

Particulate gel liquid marbles

Mizuki Tenjimbayashi,[*a,b] Ryota Tamate[c]

[a] Research Center for Materials Nanoarchitectonics (MANA), National Institute for Materials Science (NIMS), 1-1 Namiki, Tsukuba, Ibaraki 305-0044, Japan.

[b] FOREST, Japan Science and Technology Agency, Saitama 332-0012, Japan

[c] Research Center for Macromolecules & Biomaterials, NIMS, 1-2-1 Sengen, Tsukuba, 305-0047, Japan.

[*] E-mail: TENJIMBAYASHI.Mizuki@nims.go.jp.

Contents

Experimental section

Materials. Fumed silica nanoparticles AEROSIL® 300 (Evonik Industries, Germany), PDMS-modified fumed silica nanoparticles AEROSIL® RY300 (Evonik Industries, Germany), Trimethylsilyl modified fumed silica nanoparticles AEROSIL® RX300 (Evonik Industries, Germany) Liquid PDMS (DMS-T41, Gelest Inc., USA), 2-propanol (Wako, Japan) were used as received. Ultrapure water with 18.2 MΩ/cm resistance was obtained using a Direct-Q UV3 system (Merck KGaA, Germany).

Design of particulate gel (PG). PGs were obtained using a planetary ball mill (P−6, Fritsch, Germany). We added V mL of liquid PDMS, 1g of fumed silica nanoparticles, and 48 g of Zr beads (diameter 5mm) in a Zr container. The ball milling was conducted at 300 rpm for 3 minutes −1 minute interval−3 minutes reverse ratation, which was repeated for 20 cycles.

Design of particulate gel liquid marble (PGLM). We cast ultrapure water droplets in a polypropylene cup with a spoon of PGs and gently shake to cover PGs on the droplet surface. As a control, we formed LM similarly using AEROSIL® RY300.

PG structure analysis. A spoon of PGs was spread on the plastic container, and their structure was observed using digital microscopy (DSX-1000; Olympus Corporation, Japan). The particle shapes were analyzed using the software installed in this microscopy. The sample number is $N \approx 200$ for PGs with $V = 0.5$, 1.0, and 1.2 mL, and $N \approx 150$ for PGs with $V = 1.5$ mL.

The angle of repose measurement. We measured the angle of repose using the funnel method. We designed a funnel with a barely large enough diameter for PG to flow, using a 3D printer (Sonic Mini 8K, Phrozen, Taiwan). The powder mountain shape was recorded by digital camera, and Image J software processed the mountain angle evolution. We decided the plateau angle value to be the angle of repose. The sample number is $N \approx 5$ in each measurement.

Compression test. The PGLMs formed using 10 μL water droplets are sandwitched by two hydrophobic slide glasses (Microslides, Muto Pure Chemicals Co., Ltd., Japan), and compressed 80% at a rate of 0.1 mm/s using motorized one-axis stage (HPS60-20X-M5, Sigmakoki Co., Ltd., Japan). The resilience force is detected using digital microbalance (GX-203A, A&D Co., Ltd., Japan). In compression and releasing test, the glass substrate is superhydrophobized by spraying 4wt% AEROSIL® RX300 dispersion in 2-propanol. PG reconfiguration behaviors are observed using tilting digital microscope (DSX-1000, Evident (Olympus), Japan).

PDMS dynamic viscosity. The viscosity of liquid PDMS was evaluated through the steady-state shear flow measurements using a rheometer (MCR 102, Anton Paar, Austria) equipped with a cone-shaped geometry (diameter = 25 mm).

List of supplementary movies

Movie S1. Compression test

Movie S2. Compression/releasing test.

Movie S3. Impact test

Supplementary figures

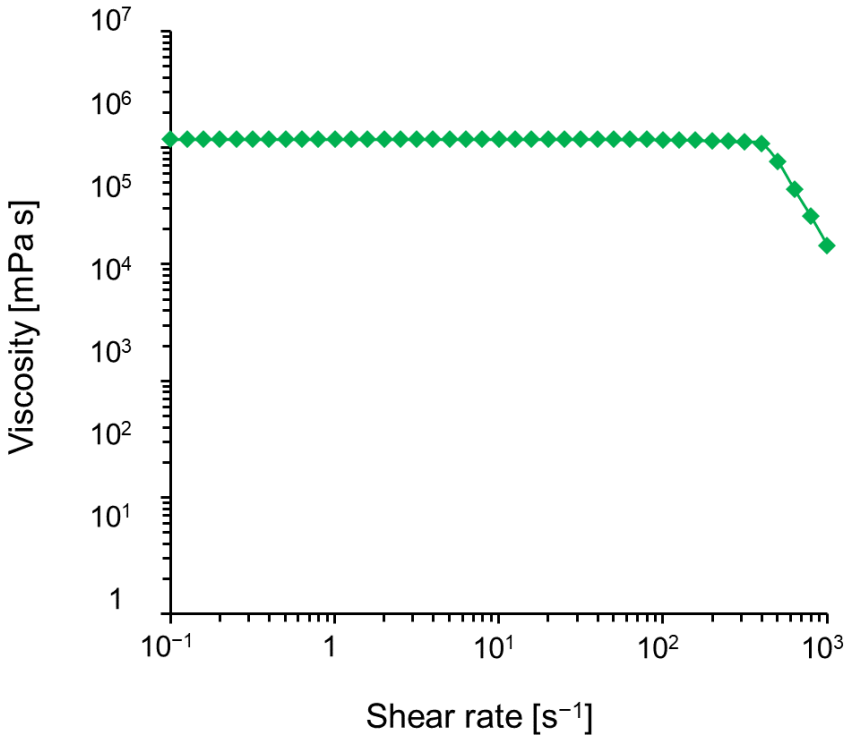

Figure S1. Dynamic viscosity of liquid PDMS.

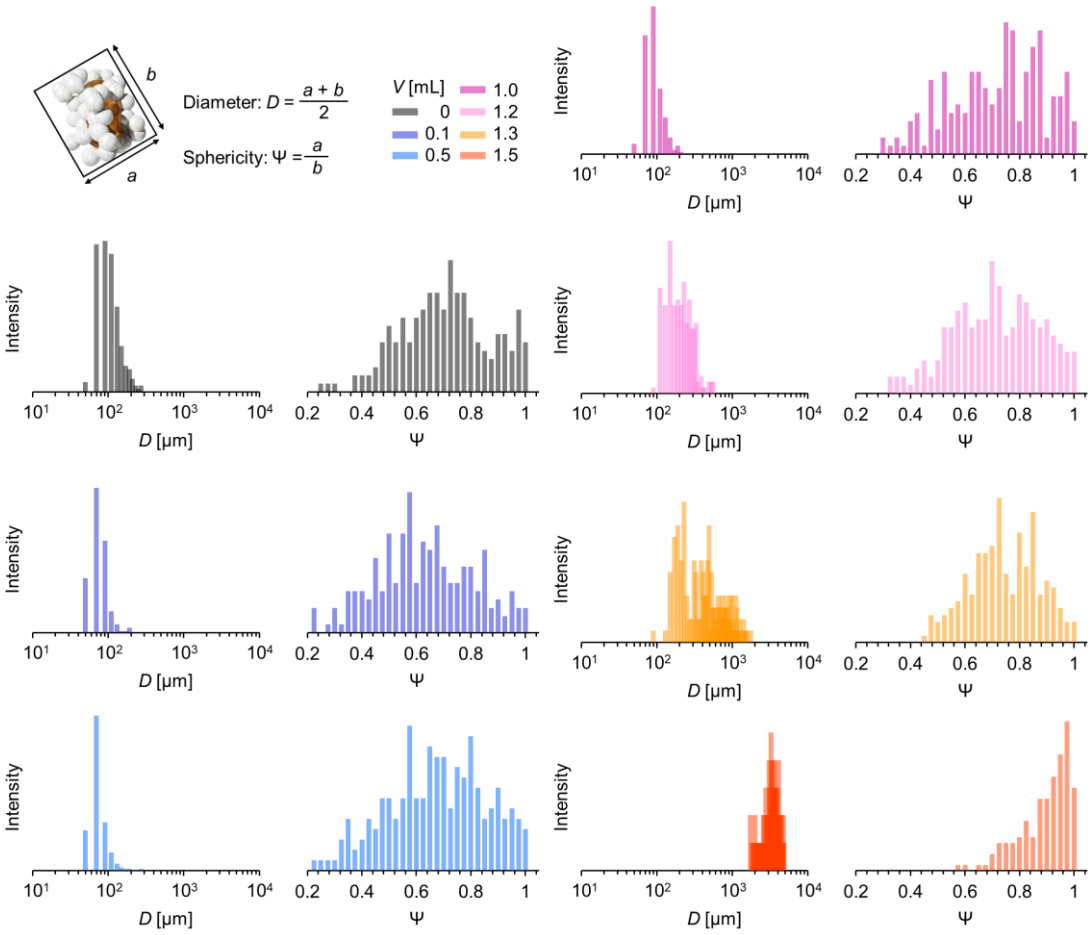

Figure S2. Histogram of PG diameter and sphericity.

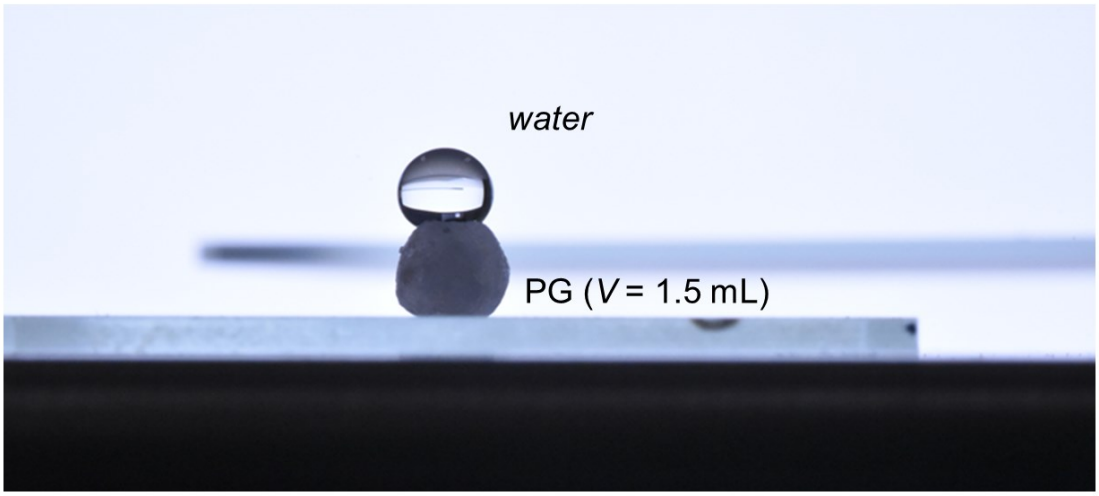

Figure S3. A photograph of water droplet sticks onto PG (V=1.5mL).

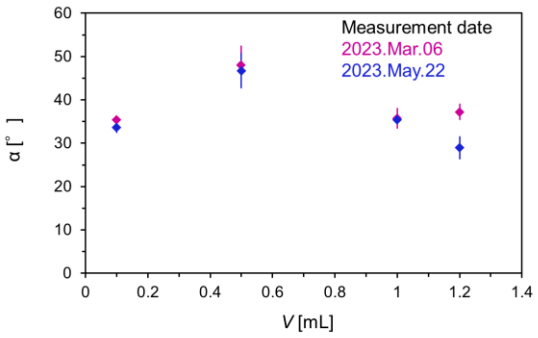

Figure S4. Long-term stability of the PGs' powder fluidity. We compared the angle of the repose evolution of PGs with different measurement dates. If PDMS spilled from the PG, the angle of the repose should be drastically increased due to its sticky properties. However, the data indicates PG kept powder fluidity even after two months.

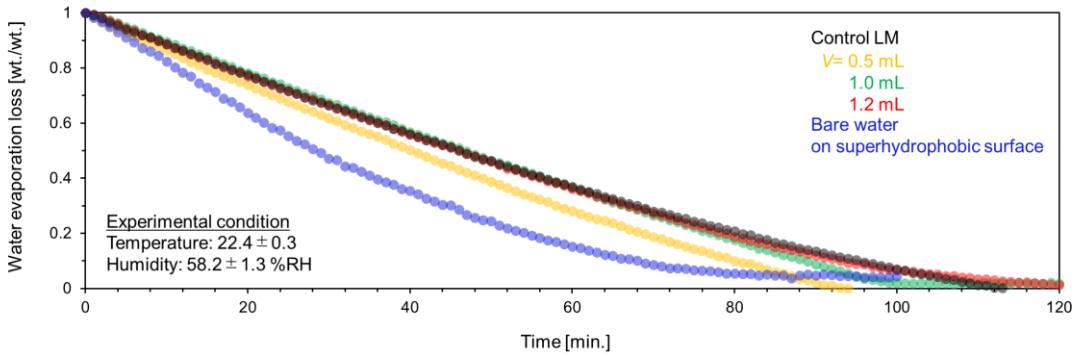

Figure S5. Comparison of water evaporation rate between a bare droplet on the superhydrophobic surface, control LM, and PGLMs. The initial water volumes were 10 μL in constant.

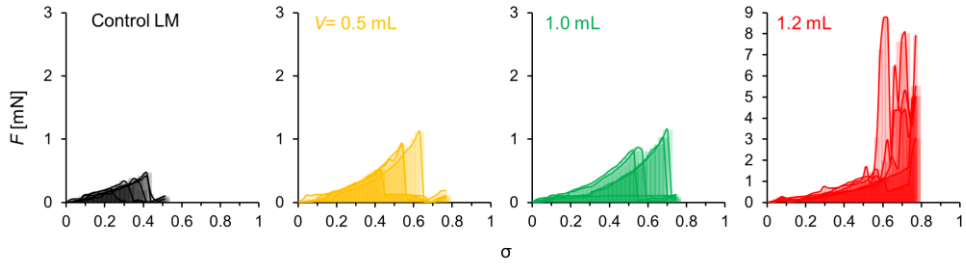

Figure S6. Compression-resilience curves of LM and PGLMs.

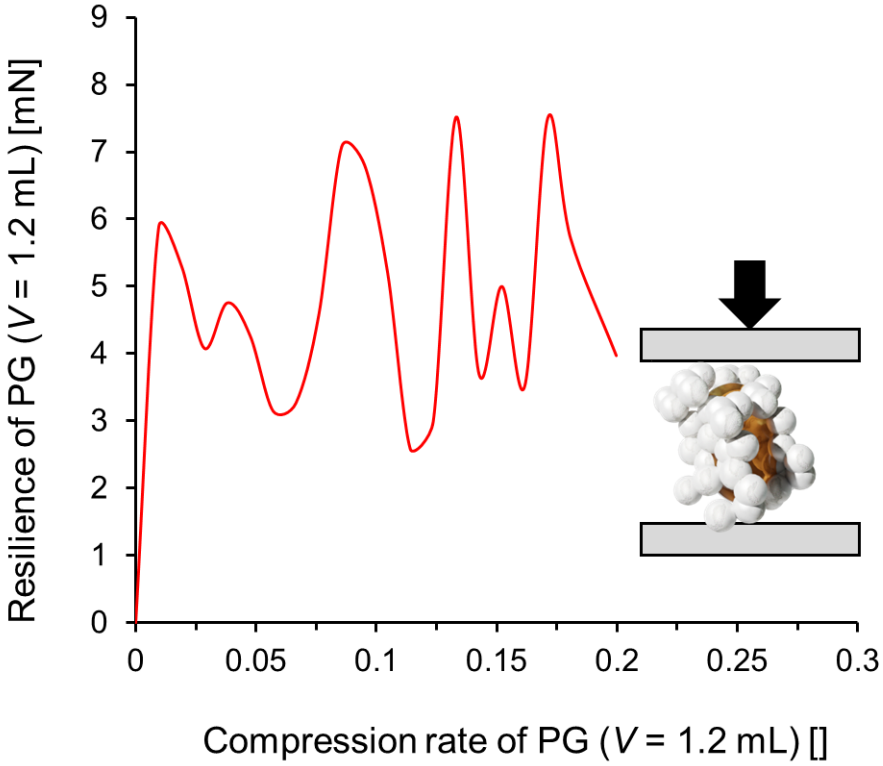

Figure S7. Compression-resilience curve of PG (1.2 mL).

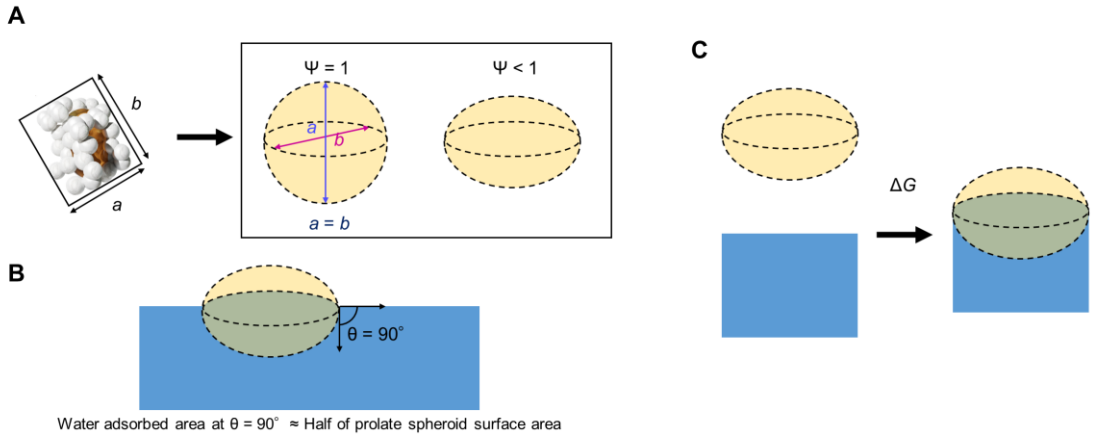

Figure S8. Estimation of the adsorption energy of the PG with different deformation. (A) We regarded the PG to be a prolate spheroid. Sphericity Ψ of the prolate spheroid expresses the deformation degree of PG. (B) Water adsorption of the prolate spheroid. When PG's Young water contact angle is 90°, the water PG interfacial area equals half of the prolate spheroid surface area. (C) Scheme of the interface formation through the adsorption of a single PG on the water surface.

Note S1. Adsorption energy of PG to the water surface

We first considered the PG a prolate spheroid (**Figure S8A**). The surface area Λ is calculated to be:

$$\Lambda = -2\pi D^2 \left[\frac{1-\Psi}{1+\Psi}\right] [-1 + \Psi^2\{1 - \tanh^{-1}(1-\Psi^2)\}]$$

where $D = (a+b)/2$ is grain diameter and $\Psi = a/b$ is the sphericity as defined in **Figure 2C**.

Then, we regarded the Young's water contact angle of PG as $\theta \approx 90°$ for model simplification (**Figure S8B**). The contact angle approximation is not inconsequent since the PG surface is covered with PDMS. In this case, the water PG interfacial area equals half of the prolate spheroid surface area 0.5Λ.

Then, we calculated the Gibbs Energy changes ΔG through PG adsorption to the water surface from the airside. In this order, we define the water and PG surface energy and their interfacial energy to be γ_L,γ_S, and γ_{SL}. The Gibbs energy change is equal to the total interfacial energy change in adsorption of PG, as seen in **Figure S8C**.

Thus, we get $\Delta G = [0.5\Lambda\gamma_S + (1–0.5\Lambda)\gamma_L + 0.5\Lambda\gamma_{SL}] – [\Lambda\gamma_S+\gamma_L] = –0.5\Lambda[\gamma_S+\gamma_L–\gamma_{SL}]$.

From Young's equation, we get

$\Delta G = –0.5\Lambda\gamma_L [1–\cos\theta] \approx -0.5\Lambda\gamma_L$.

We finally obtain

$$\Delta G \approx \gamma_L \pi D^2 \left[\frac{1-\Psi}{1+\Psi}\right] [-1 + \Psi^2\{1 - \tanh^{-1}(1-\Psi^2)\}]$$

Table S1. Summary of the critical compression and impact pressure of various LMs from the literature [S1-S8] and PGLMs.†

Particle type	Droplet	Compression pressure [Pa]	Dynamic pressure [Pa]	Reference
PTFE (35 μm)	2 wt % sodium alginate aq	156 ± 26	-	S1
PTFE (200 μm)	2 wt % sodium alginate aq	118 ± 19	-	
silica: Aerosil R812 (7 nm)	2 wt % sodium alginate aq	199 ± 22	-	
silica: Tospearl 2000B* (6 μm)	2 wt % sodium alginate aq	100 ± 16	-	
fumed fluorosilica-50% SiOH (25 nm)	2 wt % sodium alginate aq	157 ± 16	-	
fumed fluorosilica-50% SiOH (25 nm)	paraffin	93 ± 10	-	
PS particle (15μm)	water	51.4 ± 15.2	-	S2
PS particle (30μm)	water	58.6 ± 11.6	-	
PS particle (50μm)	water	73.5 ± 17.6	-	
PS particle (75μm)	water	77.8 ± 16.2	-	
PS particle (100μm)	water	81.9 ± 10.5	-	
60 μm PE particles	0.1 M KCl aq	≈ 176.4	-	S3
CaCO3 powders (particle shape)	water	≈ 73.2	-	S4
CaCO3 powders (rod shape)	water	≈ 79.6	-	
Lycopodium	water	≈ 72.5	-	S5
PTFE powder	water	≈ 41.7	-	
fluoro ppy PS (83μm)	water	-	145.2 ~ 205.3	S6
PTFE nanoparticles	water	-	95.2	S7
silica: Aerosil RX50	water	-	12.8	
silica: Aerosil RX200	water	-	47.9	
silica: Aerosil RX300	water	-	66.0	

Lycopodium	water	-	204.2	S8
PGLM 0.5mL	water	174.4	108.6 ~ 139.0	This work
PGLM1.0mL	water	174.6	172.5 ~ 257.1	
PGLM1.2mL	water	606.7	199.7 ~ 289.2	

†The compression pressure was estimated from critical resilience divided by the plate−LM contact area. The dynamic pressure was obtained from (PG)LM density multiplied by the square of critical impact velocity or critical impact height multiplied by density and gravitational acceleration constant.

[References]

S1 Z. Liu, X. Fu, B. P. Binks, and H. C. Shum, *Langmuir*, 2015, **31**, 11236–11242.

S2 Z. Liu, Y. Zhang, C. Chen, T. Yang, J. Wang, L. Guo, P. Liu, and T. Kong, *Small* 2019, **15**, 1804549.

S3 S. Asare-Asher, J. N. Connor, and R. Sedev, *J Coll Interf Sci*, 2015, **449**, 341–346.

S4 S. Azizian, S. Fujii, M. Kasahara, H. J. Butt, and M. Kappl, *Adv Powder Tech*, 2019, **30**, 330–335.

S5 A. Rendos, N. Alsharif, B. L. Kim and K. A. Brown, *Soft Matter*, 2017,**13**, 8903–8909.

S6 M. Tenjimbayashi, and S. Fujii, *Small*, 2021, **17**, 2102438.

S7 M. Tenjimbayashi, S. Samitsu, and M. Naito, *Adv Funct Mater*, 2019, **29**, 1900688.

S8 P Aussillous, and D Quéré, *Proc R Soc A: Math Phys Eng Sci*, 2006, **462**, 973–999.